Geomorphology 175–176 (2012) 126–138

Contents lists available at SciVerse ScienceDirect

Geomorphology

journal homepage: www.elsevier.com/locate/geomorph

Fluvial response to rapid episodic erosion by earthquake and typhoons, Tachia River, central Taiwan

Michelle Y.-F. Huang *, David R. Montgomery

Department of Earth and Space Sciences, University of Washington, Seattle, WA 98195-1310, USA

ARTICLE INFO

Article history:
Received 28 January 2012
Received in revised form 2 July 2012
Accepted 5 July 2012
Available online 16 July 2012

Keywords:
Landslide
Earthquake
Typhoon
Erosion
Channel response

ABSTRACT

Analysis of typhoon- and earthquake-triggered landsliding and fluvial response in the Tachia River, central Taiwan, documents highly episodic sediment supply over decade to century timescales. Landslide data from the Chi-Chi earthquake (1999) and subsequent typhoons (2001, 2004, and 2005) quantify the sediment supply from these events. Fluvial response was investigated by decadal-scale and century-scale longitudinal river profile data spanning 1904 to 2008 and by sediment delivery recorded in suspended sediment load and reservoir sedimentation data. Our results show that the different time periods of satellite images and aerial photographs used in previous studies make it difficult to unambiguously identify the causes of landslides previously attributed by some studies to the effects of the Chi-Chi earthquake rather than subsequent high intensity precipitation. In response to significant variability in sediment delivery from hillslopes, century-scale profile variation data indicate substantial bed surface elevation change of 2.6 ± 6.7 m, and decade-scale bed surface elevation change of 1.1 ± 3.3 m. Since 1993, the downstream reaches incised in response to bedload sediment trapping by reservoirs while headwater reaches aggraded in response to increased sediment delivery from uplands. A tremendous increase in reservoir sedimentation after 2000 likely reflects the effects of the highest decade-average daily rainfall since 1900. Suspended sediment load data indicate a post Chi-Chi earthquake increase in sediment concentration in low-flow events but do not exhibit the clear influence on sediment yields at higher flows as (e.g., typhoons) reported by others for fluvial response in the epicentral region.

1. Introduction

Rivers receive episodic inputs of sediment, and sediment delivery to downstream channels reflects the variable input from and transport during discrete storm events and earthquakes. Although long-term erosion rates are controlled by the broad interplay of tectonics, climate, and erosion, episodic storm events and earthquakes greatly affect the delivery of sediment to and its transport through river systems over shorter timescales. Understanding how such perturbations integrate into long-term patterns remains a central linkage between process geomorphology and landscape evolution over geologic time.

Most of the sediment delivered from unglaciated mountainous terrain originates in upstream landslides (Korup et al., 2004; Schuerch et al., 2006; Koi et al., 2008) and the linkage between upstream sediment supply and downstream channel morphology can vary over decadal to century timescales (Montgomery and Buffington, 1998). While tectonic uplift, landscape erosion, and climate change will impact channels over geological timescales, sediment supply and discharge variations resulting from extreme events (floods and droughts) or land use produce channel change over historical timescales. Over such timescales, sediment budgets are useful for linking spatial and temporal variations in sediment supply and channel response (Schuerch et al., 2006; Foster, 2010). In particular, the magnitude of century-scale channel response to variable decade-scale sediment delivery is not well constrained.

Rivers of western Taiwan are subject to episodic sediment delivery during earthquakes and frequent typhoons. In all of Taiwan, 66 large earthquakes ($M_L > 6$) occurred between 1901 and 2000, and 491 typhoons occurred between 1897 and 2010 (CWB (Central Weather Bureau) (2010)). On 21 September 1999, the Chi-Chi earthquake, the largest event in Taiwan in 60 years, happened on the Chelungpu fault ($M_W = 7.6$). It was the largest event on the Chelungpu fault in 300–620 years (Shin and Teng, 2001; Dadson et al., 2004; Hovious et al., 2011). Previous researchers have discussed how the Chi-Chi earthquake and the subsequent sequence of typhoons influenced landslide abundance, suspended sediment loads, and bedrock river incision in the epicentral region (Dadson et al., 2003; Lin et al., 2006; Cheng et al., 2007; Lin et al., 2008; Chen and Hawkins, 2009; Lee and Tsai, 2010; Yanites et al., 2010; Hovious et al., 2011). These previous studies showed that in the Choshui river catchment (river D in Fig. 1) post-earthquake suspended sediment concentrations increased for the period from 2000 to 2007 relative to the period from 1987 to 1999 (Hovious et al., 2011). Numerous investigators have found that most of the seismically produced sediment remained on

* Corresponding author. Tel.: +1 206 685 2560; fax: +1 206 543 0489.
E-mail address: michelleyfhuang@gmail.com (M.Y.-F. Huang).

0169-555X/$ – see front matter © 2012 Elsevier B.V. All rights reserved.
doi:10.1016/j.geomorph.2012.07.004

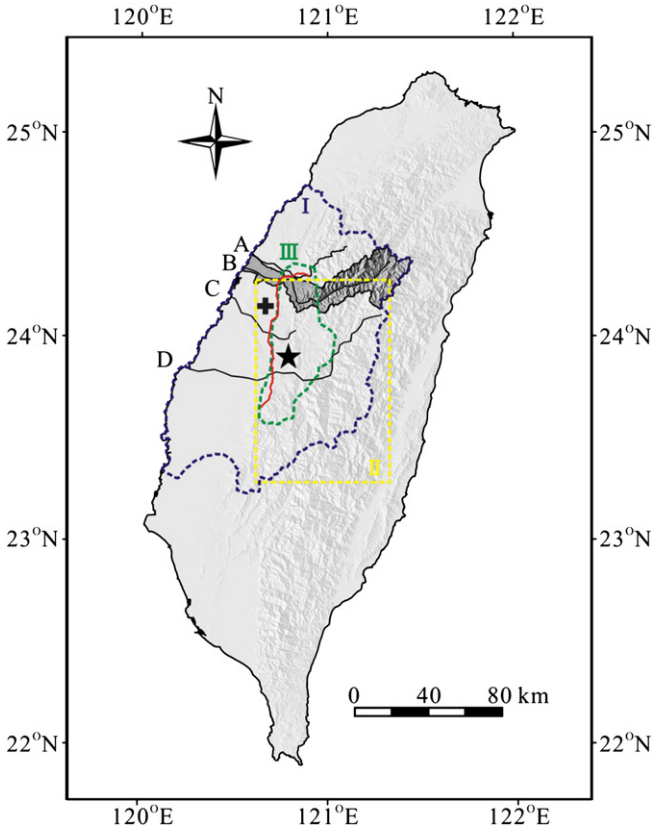

Fig. 1. The area affected by the Chi-Chi earthquake includes the basins of the Daan River (A), Tachia River (B), Wu River (C), and Choshui River (D); the epicenter of the Chi-Chi earthquake is located on the black star symbol. The Tachia River flows past Taichung city, central Taiwan (24° 8′ 35″ N, 120° 40′ 53″ E). The dark-gray area is the location of the Tachia catchment, and the cross symbol is the location of the longest running nearby rainfall station (Taichung), which provided rainfall data for Figs. 5B, 11C, 11D and 12. The study areas for previous investigations of seismically induced landslides in central Taiwan are shown by areas enclosed by dashed lines for Khazai and Sitar (2003), Wang et al. (2003), and Lin and Tung (2003), shown in areas I, II, and III, respectively.

hillslopes, and was delivered to downstream channels in subsequent typhoon events (Dadson et al., 2004, 2005; Lin et al., 2006; Chiou et al., 2007; Lin et al., 2008; Chuang et al., 2009; Hovious et al., 2011). However, long-term suspended sediment records (period 1970–1998), indicate that nine other rivers in Taiwan approached or exceeded hyperpycnal sediment concentrations before the Chi-Chi earthquake event (Dadson et al., 2005; Goldsmith et al., 2008).

Here we use landslide data, reservoir deposit data, suspended sediment data, and river profile data to examine the relative effects and impacts of climate and tectonic processes in the Tachia catchment over decadal to century timescales. We also reassess studies of the landslide response of the Tachia River to the 1999 Chi-Chi earthquake and subsequent typhoons in relation to river response to variations in sediment supply.

2. Study area

The Tachia River is located in central Taiwan (Fig. 1) at the north end of the surface rupture during the Chi-Chi earthquake and flows 124 km westward from its source in the Central Mountain Range, dropping over 3700 m to the river mouth. Within the 1244-km^2 catchment, the local climate varies from temperate to subtropical with annual average rainfall of 2725 mm (Basianshan rainfall station, 1420P081), as determined from the Water Resources Bureau (WRB) Hydrological Yearbooks for the period 1989–2010. The annual average temperature varies between 14.6 and 22.6 °C, and the river's discharge averages 32 m^3 s^{-1} in the dry season (April to September) and 98 m^3 s^{-1} in flood season (October to March) (station I in Fig. 2B) (WRAP, 2005). Bedrock varies in age from Eocene to Quaternary (Fig. 2A). Eocene strata consist of argillite, sandy shale sandstone, slate and phyllite. Oligocene rocks include sandstone, shale, quartzite, slate and coaly shale. The upstream Miocene strata consist of argillite, sandy shale sandstone. The downstream Miocene strata consist of sandstone, mudstone and shale. Pliocene strata consist of poorly consolidated sandstone and siltstone/mudstone. Quaternary strata include fluvial terrace deposits and recent alluvium. The Tamaopu-Shungtung fault separates Miocene and Quaternary-age strata, and five active faults (Chelungpu, Sanyi, Tuntzuchiao, Tienchanshan and Tachia faults) cut strata of Quaternary-age.

The drainage basin of the Tachia River is an area rich in water and natural resources. Six reservoirs (Fig. 2B) and seven hydropower plants generate 25 hundred million kilowatt hours annually (Bureau of Energy, Ministry of Economic Affairs, 2009). In the upper reaches of the river, where the population density is just 10 people per square kilometer, land use includes the Formosan Landlocked Salmon Refuge, national parks, watershed protection areas, orchards, and farms (WRAP, 2010). In the middle reaches, population density is as high as 500 people per square kilometer; and population density reaches 4000 people per square kilometer in the downstream region (WRAP, 2010). A series of bridges, levee embankments, and roads intersect and locally constrain the lower and middle reaches of the river.

Located at the collision of the Eurasian and Philippine Sea plates, Taiwan experiences frequent earthquakes (Wu et al., 1997). Since recording of earthquake activity began in 1898, seven earthquake events have occurred with magnitudes >5 in central Taiwan (WRAP, 2010). After a 6.1-magnitude earthquake in 1909, four additional earthquakes with magnitudes from 5.5 to 6.8 occurred from Aug. 1916 to Jan. 1917. In 1935, several thousand people were killed in the magnitude 7.1 Hsinchu-Taichung earthquake when the Tuntzuchiao fault shifted 2 m right and 0.6 m vertically (WRAP, 2010). According to CWB records, the Chi-Chi earthquake (1999, Mw = 7.6) was the largest earthquake to strike the Tachia catchment from 1901 to 2010. The 7.6-magnitude Chi-Chi earthquake struck central Taiwan when offset along the Chelungpu fault caused 9 m maximum horizontal displacement and 15–16 m maximum vertical displacement (Lee et al., 2005). In the Tachia catchment, the fault rupture raised Shih-Kang reservoir and Bei-Fung bridge 9.8 and 8 m, respectively (Chen and Hawkins, 2009). According to the Soil and Water Conservation Bureau Chi-Chi earthquake landslide database (SWCB, 2000), this earthquake caused 14,000 ha of landslides near the Chelungpu fault (Wang et al., 2003).

Typically, three to four tropical cyclones (typhoons) strike Taiwan each year during July to September, from the north Pacific and South China Sea (CWB, 2010). Heavy rainfall during numerous typhoons occurred in the Tachia catchment between the start of discharge records in 1897 and the 1999 Chi-Chi earthquake. According to WRAP (2010), major flooding occurred along the Tachia River in 1959, 1963 (typhoon Gloria), and 1981 (typhoon Maury). After the Chi-Chi earthquake, typhoon events caused widespread landsliding and serious damage during typhoons Toraji, Mindulle, Aere, and Haitang (Chiou et al., 2007). The maximum daily rainfall and three-day cumulative rainfall recorded in the Shinbogong rainfall station records (point G in Fig. 2B) are presented in Table 1. The occurrence of frequent storm events and strong earthquakes in the same catchment provides an opportunity to investigate catchment-scale response to climate-driven impacts and tectonic activity over decadal to century timescales.

3. Landslides

3.1. Previous studies in the Tachia catchment

3.1.1. Sources of landslide data

Previous studies used four landslide data sources for the Chi-Chi earthquake and subsequent typhoon events. Different studies have

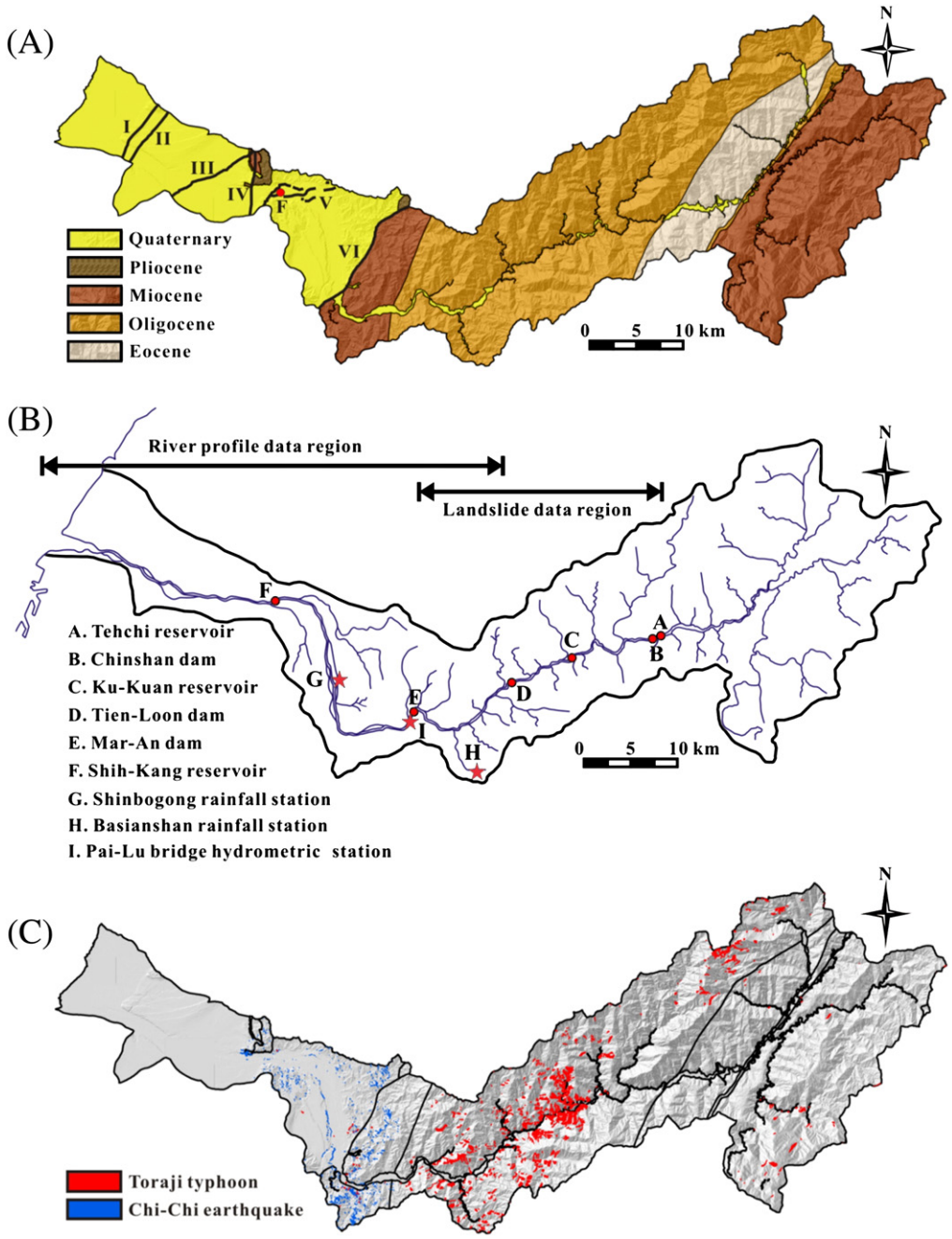

Fig. 2. Characteristics of the Tachia River basin. (A) Generalized geological map showing age of rock units. It also shows six active fault lines (black lines): I = Tachia fault, II = Tienchanshan fault, III = Tuntzuchiao fault, IV = Sanyi fault, V = Chelungpu fault, and VI = Tamaopu-Shuangtung fault. (B) Locations of six dams and associated reservoirs and three meteorological stations along the river, and the extent of the regions investigated for landslides by river subcatchment and for historical river profile data. (C) Locations of landslides in the SWCB (Soil and Water Conservation Bureau) Chi-Chi earthquake (blue) and Toraji typhoon (red) landslide database within the drainage basin of the Tachia River; black lines show the lithological boundaries from panel A.

relied upon different data sets. Lin et al. (2000) and Khazai and Sitar (2003) used CEDAMS (Chi-Chi earthquake Database Analysis and Management System) from the National Center for Research on Earthquake Engineering (NCREE). The SWCB database for the Chi-Chi earthquake was used by Lin and Tung (2003), Wang et al. (2003), and Chen (2009); and Wang et al. (2003) and Chen (2009) used the SWCB Toraji typhoon database (SWCB, 2002). In addition to these sources, Chen (2009) also used the Central Geology Survey (CGS) Mindulle typhoon database. Other studies have used various SPOT satellite images and 1:5000 aerial photographs to map landslides in the Tachia catchment (Cheng et al., 2006; Chiou et al., 2007; Chen and Hawkins, 2009; Chuang et al., 2009).

The CEDAMS and SWCB databases were produced by government agencies and verified with field investigations (Khazai and Sitar, 2003; Lin and Tung, 2003; Wang et al., 2003). Both databases were developed from analysis of Spot satellite images and 1:15,000 aerial photographs, taken on 24 July 1999 and 27 September 1999, to identify 10,000 seismically induced landslides in the Chi-Chi earthquake event. The effective mapping resolution of the SWCB database is 6.25 m (Chen, 2009). The CGS Mindulle database used Formosat-2 remote sensing images acquired in 2004, with an effective mapping resolution of 2 m (Chen, 2009).

3.1.2. Previous detection

Khazai and Sitar (2003), Lin and Tung (2003), and Wang et al. (2003) used CEDAMS and SWCB databases to map landslides in three different study areas (Fig. 1, areas I, II, III, respectively). All three studies

Table 1
Daily and accumulated 3-day rainfall intensity for major typhoon events in the Tachia River and recorded since the Chi-Chi earthquake at the Shinbogong rainfall station.[a] Data from Water Resources Bureau Hydrological Yearbooks.

Events	Time period	Max. daily rainfall [mm]	3-day rainfall accumulation [mm]
Toraji	7/28–31/2001	234	239
Mindulle	6/28–7/3/2004	618	1000
Aere	8/23–26/2004	314	411
Haitang	7/16–20/2005	312	335

[a] The location of this station is shown as point G in Fig. 2B.

Table 2
Time intervals covered in of the source images used to derive of landslide databases.

	SPOT image time	Aerial photographs time
Before Chi-Chi earthquake	4/1/1999	12/21/1997–9/10/1999
Chi-Chi earthquake (9/21/1999)	10/31/1999	10/31/1999–12/9/2000
Toraji typhoon (7/28–31/2001)	11/18/2001	8/14/2001–2/21/2003
Mindulle typhoon (6/28–7/3/2004)	7/21/2004	7/7/2004–7/31/2004
Haitang typhoon (7/16–20/2005)	10/12/2004	1/21/2005, 8/1/2005–1/21/2006

found that seismically induced landslides (Keefer, 1984) were closely related to areas of high peak ground acceleration (PGA), with areas of greatest damage close to the epicenter or main fault offset (Khazai and Sitar, 2003; Lin and Tung, 2003; Wang et al., 2003; Meunier et al., 2007). Most of the seismically induced landslides were shallow landslides and their spatial distribution was not associated with particular geological units (Lin et al., 2000; Khazai and Sitar, 2003). According to these two earthquake databases, the coseismic landslides in the Tachia catchment were located downstream of the main range-bounding fault (see Fig. 2C, blue areas). Meunier et al. (2007) analyzed the seismically induced landslides in the Choshui catchment in the epicentral region and found that the density of Chi-Chi earthquake landslides was linearly and highly correlated with vertical and horizontal components of PGA. Chen (2009) analyzed landslide response to the Chi-Chi earthquake (1999) and Toraji typhoon (2001) using the SWCB database and the Mindulle typhoon (2004) using the CGS database. He reported a high density of seismically induced landslides in argillite, slate, and phyllite strata between Tehchi reservoir and Mar-An dam, well upstream of the areas of seismically triggered landsliding reported in the CEDAMS database.

Cheng et al. (2006) and Chiou et al. (2007) used 6.25 m resolution SPOT satellite images, 1:5000 aerial photographs, and NDVI (Normalized Difference Vegetation Index) to produce high resolution Chi-Chi earthquake (1999), Toraji typhoon (2001), Mindulle typhoon (2004), and Haitang typhoon (2005) landslide maps for the Tachia catchment, with a minimum distinct landslide area of 1000 m^2. They also digitized aerial-photograph-based topographic maps to generate multitemporal DEMs and used local differences in elevation between these DEMs to evaluate landslide volumes for different events. They then used these data in the program HEC-6 to estimate sediment transport through the Tachia River and concluded that the river channel elevation will rise up 20 m at Chinshan dam after 2005 with as much as 40% of the landslide-delivered sediment remaining in this area. Cheng et al. (2006) and Chiou et al. (2007) also linked high suspended sediment concentrations with a post-earthquake effect. Notably, however, according to their reported image acquisition times (listed in Table 2), their mapping of seismically induced landslides includes periods of high intensity rainfall (Fig. 3). Specifically, their image acquisition period for mapping landslides associated with the Chi-Chi earthquake event (from April 1999 to December 2000, as shown in Fig. 3, time period II), included 13 days with rainfall exceeding 100 mm, according to the Basianshan rainfall station (point H in Fig. 2B). Consequently, these studies may have considered landslides triggered by high intensity typhoon rainfall as seismically induced, and thus the number of landslides attributed to the Chi-Chi earthquake is a maximum value that we will refer to as 'post-earthquake period' landslides (PEL).

Chen and Hawkins (2009) and Chuang et al. (2009) used 10- and 20-m-resolution SPOT satellite images, and 1:5000 aerial photographs to generate for the Tachia catchment 20-m-resolution landslide maps for Herb typhoon (1996), Chi-Chi earthquake (1999), Toraji typhoon (2001), and Mindulle typhoon (2004). They found that earthquake-attributed landslides occurred where PGA exceeded 200 cm s^{-2} and most of the seismic landslides were located between Tehchi reservoir and Mar-An dam. Chuang et al. (2009) also surveyed sediment discharge of the Tachia River from 1979 to 2003. They concluded that although flow discharge during typhoon Toraji (2001) was less than that of typhoon Herb (1996) the sediment discharge of typhoon Toraji (2001) was doubled than that of typhoon Herb (1996), an effect they attributed to the influence of the Chi-Chi earthquake. However, neither study (Chen and Hawkins, 2009; Chuang et al., 2009) reported the time period covered by the images used to map landslides.

The mapping of earthquake-attributed landslides in different regions of the Tachia catchment depended on images covering different time periods to map landslides and came to differing conclusions. As illustrated in Table 3, Khazai and Sitar (2003), Lin and Tung (2003), and Wang et al. (2003) all used images spanning a short time period around the Chi-Chi earthquake (period I in Fig. 3) and concluded that most seismically induced landslides occurred near the Chelungpu fault. The different conclusions of Cheng et al. (2006) and Chiou et al. (2007) were based on analysis of images obtained over a longer time period before and after the Chi-Chi earthquake (period II in Fig. 3). In contrast to earlier studies, they proposed that numerous seismically-induced landslides were clustered between Tehchi reservoir and Mar-An dam. We thus suspect that the latter studies included landslides that were triggered by periods of intense precipitation following the earthquake.

3.2. Data

Because of high resolution landslide maps and the clear image acquisition period, we analyzed in more detail the landslide database published by Cheng et al. (2006) and Chiou et al. (2007), which includes landslides from the Chi-Chi earthquake (1999) and landslides between Tehchi reservoir and Mar-An dam that occurred during typhoons Toraji (2001), Mindulle (2004), and Haitang (2005). Unfortunately, these maps do not distinguish source areas from deposition areas for individual landslides. The study area and image acquisition periods are illustrated in Fig. 2B and Table 2. Within this 396-km^2 area there are 44 subcatchments located between Tehchi reservoir and Mar-An dam (Fig. 2B) and over 5000 landslides larger than 1000 m^2 are included in the multievent data set for the region between Tehchi reservoir and Mar-An dam. Data in the serial landslide database include the total landslide area and volume and the average pre- and post-failure elevation difference for the landslides in each subcatchment. The volume and average elevation difference were evaluated from multitemporal DEMs generated from stereo aerial photographs (Cheng et al., 2006; Chiou et al., 2007).

The DEMs were created by digitizing contours from 1:5000 (0.25-m resolution) photo base maps published by the Aerial Survey Office (Forestry Bureau, Taiwan Council of Agriculture) with contour intervals of 5 and 10 m, respectively, for lowlands (elevations < 1000 m) and higher mountain regions (elevations > 1000 m). After digitizing the elevation of these photos and converting to a raster-based map, ArcGIS Spatial Analyst Cut/Fill tool was used to evaluate volume and elevation differences between the two maps (Cheng et al., 2006;

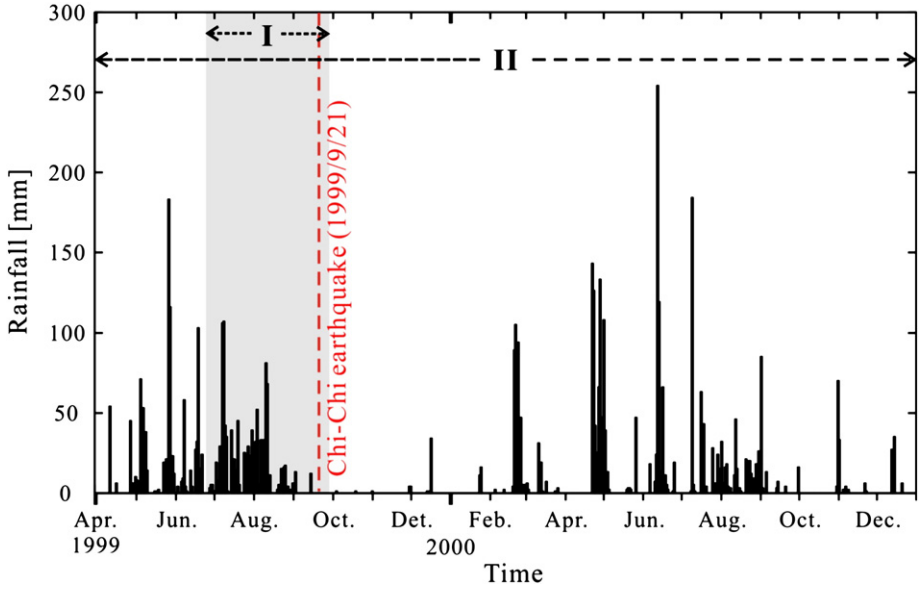

Fig. 3. Daily rainfall records of mountain region Basianshan rainfall station (TWD67, location shown in Fig. 2B) for the period of 1 Apr. 1999–31 Dec. 2000, time period II of Table 3, covered by images used in mapping for the Chi-Chi earthquake landslide database. Gray band shows the time period covered by images used to prepare the SWCB and CEDAMS Chi-Chi earthquake landslide databases (period I of Table 3).

Chiou et al., 2007). The elevation error of these multitemporal DEMs was estimated to be 0.5 m (Cheng et al., 2006).

3.3. Results

3.3.1. Landslide density ratio

We used the landslide density ratio (LD) to evaluate the extent of landsliding within individual subcatchments. The LD is calculated as the ratio of subcatchment landslide area to the drainage area of the subcatchment. It thus quantifies the relative extent of landsliding in the different subcatchments. Typhoon Mindulle (2004) triggered the largest area of landslides during the highest intensity rainfall recorded in this area. The highest LD, $LD_{max}=38\%$, occurred during Mindulle typhoon (2004) and the average LD for all 44 tributaries was also the highest in this event, $LD_{average}=7.8\%$. The minimum LD value in this event also was the highest of those in the four events. The second highest LD value is for PEL associated with the Chi-Chi earthquake, $LD_{max}=35\%$ and $LD_{average}=7.5\%$. The smallest LD_{max} value (32% with $LD_{average}=6.1\%$) was produced in Toraji typhoon (2001), which had the lowest rainfall intensity. Smaller subcatchments (<10 km^2) exhibited substantial variability in LD, whereas LD values for larger subcatchments were less variable over the four events (Fig. 4A).

Table 3
Different Chi-Chi earthquake landslide data sources were from different satellite images and the time period of aerial photographs of previous studies.

Densest landslide region		Image period	Database name	Reference
Downstream	Upstream			
√		I	CEDAMS	Khazai and Sitar (2003)
√		I	SWCB	Lin and Tung (2003)
√		I	SWCB	Wang et al. (2003)
	√	II		Cheng et al. (2006)
	√	II		Chiou et al. (2007)
	√	I	SWCB	Chen (2009)

The downstream landslide area means near the Chelungpu fault region, and the upstream area means the region between Tehchi reservoir and Mar-An dam. Image acquisition periods I and II are shown in Fig. 3.
√ means region is covered by images used.

3.3.2. Equivalent landslide erosion

We estimated cumulative landslide volumes from catchment-wide landslide areas using the global data compiled by Larsen et al. (2010). All catchments plot close to the 1-m average depth line for soil landslides in the global data compilation (Fig. 5A), indicating a dominance of shallow-regolith landsliding over deep-seated bedrock landslides. According to the 44 subcatchment elevation differences from multitemporal DEMs, the total average elevation difference of our data, 0.75 m, is close to Larsen et al.'s (2010) global average for soil landslides. We therefore conclude that the landslide volume data is reasonable even though the erosion rates implied by the total volumes of these landslides are quite high. As another check, we evaluated the total landslide volumes, and thus the implied subcatchment erosion rates, by the product of total landslide area and average elevation difference and found the reported total volumes to be a little lower and therefore more conservative. We therefore used these values (total subcatchment landslide volume divided by subcatchment area) to evaluate subcatchment-scale landslide erosion (LE) in different events.

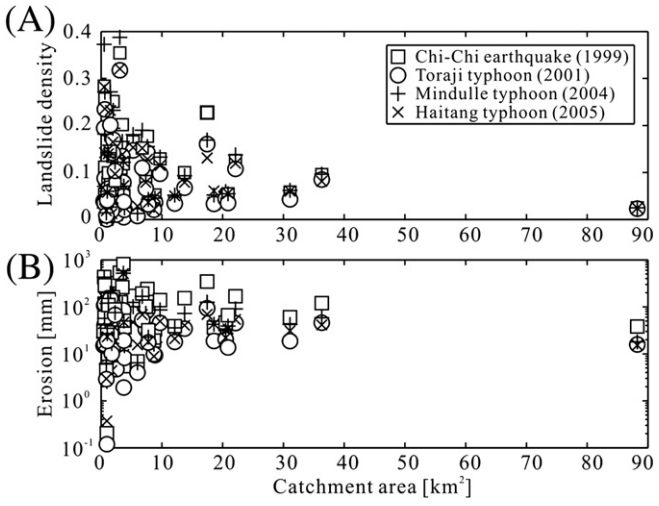

Fig. 4. (A) The relationship between landslide density ratio (LD) and subcatchment area within 44 tributaries, with four landslide events shown in different symbols. (B) The relationship between the equivalent landslide erosion (LE) and catchment area.

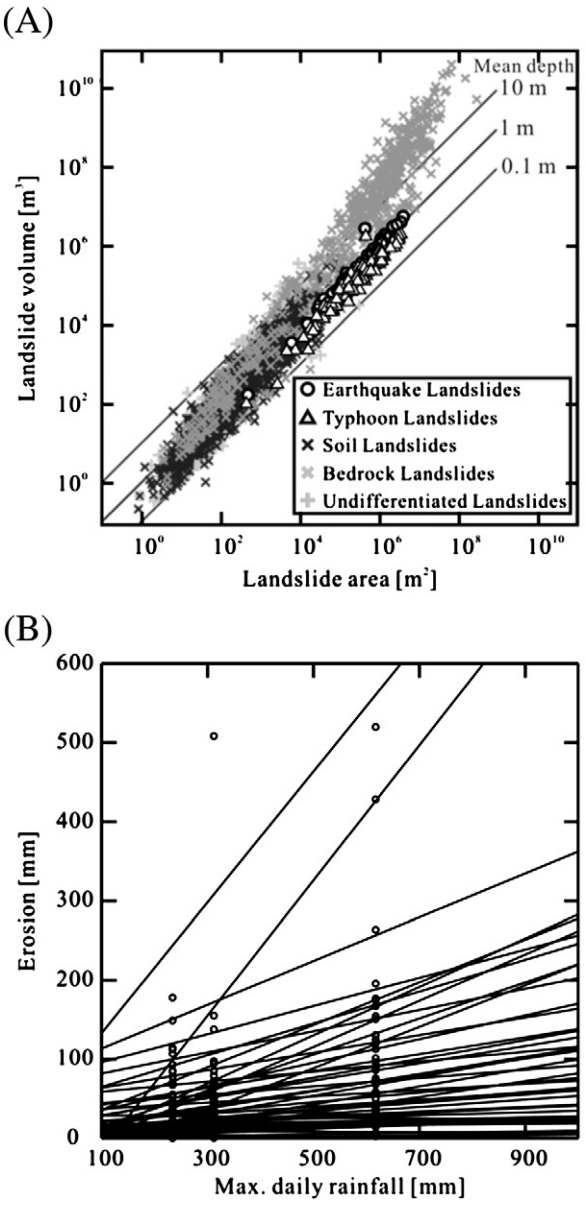

Fig. 5. (A) Comparison of landslide volume evaluated from multitemporal DEMs for earthquake- and typhoon-triggered landslides (circle and triangle symbols, respectively) overlain on data from Larsen et al. (2010). (B) Variation of landslide erosion rate of 44 subcatchments in relation to maximum daily rainfall records from Shinbogong rainfall station (Table 1) during three typhoon events. The black lines show linear regression fit results for individual subcatchments.

We used total subcatchment landslide volumes to evaluate subcatchment landslide erosion rates, LE, for each event. As for subcatchment LD values, the LE values for smaller subcatchments (<10 km^2) varied greatly, with LE values for larger catchments being similar for all four events (Fig. 4B). Notably, the average LE of PEL associated with the Chi-Chi earthquake was the highest among the four events, with $LE_{PEL} = 101.8$ mm. Although the LE values in different subcatchments and events that show most of the high LE regions are close to the main river channel, no clear pattern linked variations in LE with the spatial distribution of these subcatchments. Rock strength properties in this area (reviewed by Chuang et al., 2009) show no correspondence between rock strength and the LE of earthquake or typhoon events, although differences in weathering and near-surface fractures may help explain patterns of earthquake and typhoon-induced landsliding (as we discuss further later).

To investigate the relationship between rainfall intensity and landslide erosion rate (Fig. 5B), we used erosion rate data from 44 subcatchments and maximum daily rainfall data of Shinbogong rainfall station (Table 1) of three typhoon events (Toraji (2001), Mindulle (2004), and Haitang (2005)) to fit a simple linear regression for each subcatchment. The data from individual basins showed strong correlation between LE and maximum daily rainfall, as 42 out of 44 subcatchments displayed a significant positive linear relationship; and the regressions for over half of the catchments had correlation coefficients (R^2 values) > 0.8. In all but two subcatchments (both of which had low LE values), higher rainfall systematically translated into more landslides. The wide range of regression slopes apparent in Fig. 5B indicates that different subcatchments have differing propensity to produce landslides in response to precipitation and thus that some areas are more sensitive to the impact of rainfall intensity.

4. River response

4.1. Previous studies of the Tachia River

The Tachia River is located at the north end of the Chelungpu fault, which passes through the downstream region of the river at Shih-Kang reservoir (see Fig. 2B, location F). After the 1999 Chi-Chi earthquake, researchers investigated fault zone activity using historical data (Sung et al., 2000; Chen et al., 2006), fluvial terrace development (Chen et al., 2003), and structural geology (Lee et al., 2005; Yue et al., 2005; Lee and Chan, 2007) along the Tachia River. Chen et al. (2003) used aerial photographs, 1:5000 topographic maps, and GPS measurements to evaluate river terrace elevation differences between various faults of the Tachia River. They found that, in the fold-thrust belt of the frontal western foothills, the Tachia River flowed above a tectonic ramp structure, as also proposed by Lee et al. (2005). Sung et al. (2000) and Chen et al. (2006) used the 1904 version of Taiwan Bautu (1:20,000 scale) and the 1985 topographic map (1:25,000 scale) to study the Hack (1973) stream-gradient index (SL index). According to their investigations, high local SL indices on the 1904 map reflect fault activity of the Chelungpu, Tuntzuchiao, and Shungtung faults (see Fig. 2A), and the 1985 SL index curve is much smoother than in 1904, except for the Tuntzuchiao fault where offset occurred during the magnitude 7.1 Hsinchu-Taichung earthquake in 1935 (fault III in Fig. 2A) (Sung et al., 2000).

4.2. Data

Published reports of the Taiwan Water Resources Agency include monitoring data from 134 channel cross sections surveyed at intervals of about 0.5 km along the channel (Figs. 2B and 6A) following Taiwan government standards (Shen, 1994). Of the cross sections, 99 were surveyed repeatedly between 1993 and 2008; 35 additional cross sections were measured in upstream districts between 2003 and 2008. Cross section locations are marked by steel or concrete piles at both ends of the cross section and the locations of these piles are determined by benchmark and GPS. Historical longitudinal profile data from the year 1904 (WRAH, 2010) was based on a historical map, known as Taiwan Baotu, published by Japanese authorities in 1904. This map was digitized by ASCC GIS lab (Academia Sinica Computing Center) in 2003 and readjusted spatially to a recent DEM (year 2000, published by the Department of Interior, ROC) (Sung et al., 2000; Chen et al., 2006). The river bed profile elevation data was obtained by normalizing the lowest elevation data across each cross section, following Taiwan government standards (Shen, 1994). In addition, channel grain size data was collected in 16 cross sections in 1983 and 22 cross sections in 2008, and channel width data was measured from 1:5000 aerial photographs for 87 cross sections in four years (1998, 2000, 2005, and 2008).

Sediment volume data were also published for six reservoirs in WRAP series reports. The six reservoirs in the Tachia River, from upstream to downstream (Fig. 2B), include Tehchi reservoir (drainage area 592 km^2,

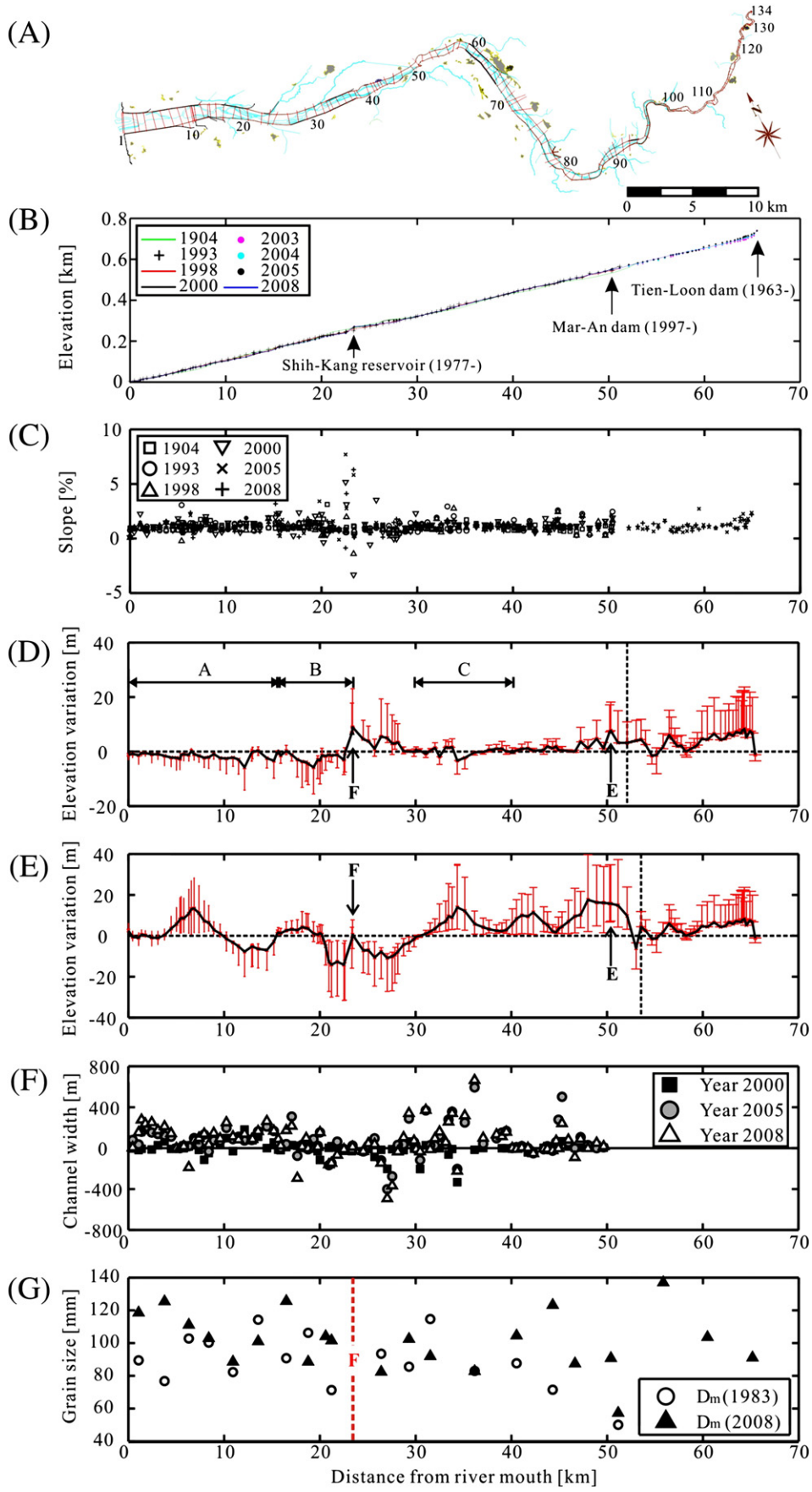
(A)
1
10
20
30
40
50
60
70
80
90
100
110
120
130
134
N
0
5
10 km
(B)
Elevation [km]
1904
1993
1998
2000
2003
2004
2005
2008
Tien-Loon dam (1963-)
Mar-An dam (1997-)
Shih-Kang reservoir (1977-)
(C)
Slope [%]
1904
1993
1998
2000
2005
2008
(D)
Elevation variation [m]
A
B
C
F
E
(E)
Elevation variation [m]
F
E
(F)
Channel width [m]
Year 2000
Year 2005
Year 2008
(G)
Grain size [mm]
F
Dm(1983)
Dm (2008)
Distance from river mouth [km]

built in 1973), Chinshan dam (drainage area 596 km^2, built in 1970), Ku-Kuan reservoir (drainage area 686 km^2, built in 1961), Tien-Loon dam (drainage area 827 km^2, built in 1963), Mar-An dam (drainage area 916 km^2, built in 1997), and Shih-Kang reservoir (drainage area 1061 km^2, built in 1977). Reservoir sediment data have been monitored since they were constructed. Sediment data for these reservoirs are estimated by the water storage loss between the date of construction and subsequent capacity estimates based on bathymetric resurvey.

To evaluate the volume of fluvially transported sediment, we also collected the available hydrometric station data along the Tachia River (Pai-Lu bridge station, 1420H037) from the Water Resources Bureau (WRB) Hydrological Yearbooks for the period 1978–2003. In these data, water discharges were measured daily and suspended sediment concentrations were measured for 30 samples per year. These samples used a depth-integrating, suspended-sediment sampler (DH-48) and were calibrated annually by WRB (Kuo and Liu, 2001). We collected aerial photographs from three years to investigate channel migration within three segments of the monitored channel in 1975, 1988, and 2005 (locations of these segments are shown in Fig. 6D). The aerial photographs, published by the Aerial Survey Office of the Taiwan Forestry Bureau, have a resolution of 0.25 m.

4.3. Results

4.3.1. Longitudinal profile of the main river channel

The low degree of concavity and relatively straight longitudinal profile constructed from 134 cross sections of the Tachia River locations contrasts with the typical concave form of river longitudinal profiles (Fig. 6A and B). The slopes for each surveyed section of the river are all close to 1%, except for near Shih-Kang reservoir where offset during the Chi-Chi earthquake created a pronounced knickpoint (Figs. 6C and 7). The strikingly uniform slope of this river suggests a high sediment load and implies a transport-limited state (Snow and Slingerland, 1987; Rãdoane et al., 2003; Chen et al., 2006; Lee and Tsai, 2010).

4.3.2. Seismic-knickpoint of the Tachia River

During the Chi-Chi earthquake, major surface offset produced a knickpoint at the Shih-Kang reservoir (see Figs. 6B and 7) resulting in vertical displacement of up to 11 m. Another surface rupture zone is located along the Tingpu fault (location C in Fig. 7). As of 2008, the Shih-Kang reservoir section still exhibits an abrupt change in gradient, and a new (post-2000) delta is forming because of the backwater effect upstream of the Shih-Kang reservoir. Based on surveyed bed elevation profiles, the incision rate at this knickpoint was 1 m y^{-1} for the period from 2000 to 2008. An additional knickpoint in the longitudinal profile surveyed in 1904 at the location of Sanyi fault (point A in Fig. 7) had been eroded by the 1993 survey, indicating a century-scale local incision rate of about 0.2 m y^{-1}. According to an interpretive geological cross section (Yue et al., 2005), researchers have proposed that a bedding-parallel Chelungpu-Sanyi thrust system merges at depth with the Chelungpu fault along the Tachia River (Lee et al., 2005; Yue et al., 2005). Interpreting the knickpoint at location A on the 1904 profile as reflecting nineteenth century offset on the Sanyi fault is consistent with other independent evidence for offset along the Chelungpu fault in the nineteenth century reported by Chen et al. (2001).

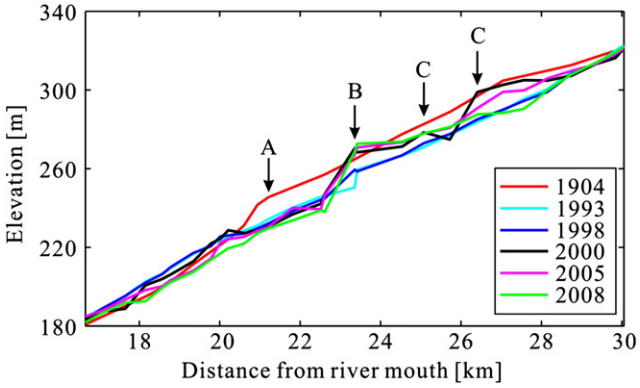

Fig. 7. Tachia River channel profile near the 1999 earthquake-generated knickpoint at Shih-Kang reservoir section (location B). The surface rupture zone of Chi-Chi earthquake involved the Chelungpu fault (location B) and two strands of the Tingpu fault (locations C). The Sanyi fault is located at the inflection on the 1904 profile (location A).

4.3.3. Decadal-scale and century-scale bed elevation variations

Despite the overall uniform slope, the cross-sectional data reveal substantial decadal-scale and century-scale local variance in bed surface elevation normalized relative to the 1993 and 1904 profiles (Fig. 6D and E). Upstream of the extent of the 1904 survey (53 km), elevations are normalized to riverbed elevation data from 2003. Likewise, upstream of the extent of the 1993 survey (51 km), elevations are normalized to riverbed elevation data from 2003.

Decadal-scale (1993 to 2008) variability of the river elevations shows a normal distribution with a mean of 1.1 m aggradation and a standard deviation of $\pm$3.28 m (Fig. 8A). Century-scale (1904 to 2008) bed elevation exhibits a mean of 2.6 m aggradation and a standard deviation of $\pm$6.67 m (Fig. 8B). According to these normalized distributions, over the past two decades channel elevation response to perturbations in sediment supply is about half the amplitude of century-scale variations. This high degree of recent variability suggests that the Tachia River is highly responsive to a recent increase in sediment supply.

Riverbed elevations in the upper and lower river differ in their decadal-scale variability (Fig. 6D), with several distinct zones of response. The lowermost reaches of the river, from the river mouth to Shih-Kang reservoir (0 to 23 km), exhibit consistent incision. In the vicinity of the Shih-Kang reservoir (location F in Figs. 2B and 6D), the surface offset from the Chi-Chi earthquake is apparent in the dramatic bed elevation variability. In the middle reaches (28 to 47 km), the channel bed exhibited little variability, reflecting a dominantly transporting zone. The channel bed systematically aggraded in the basin headwaters (47 to 66 km).

In the vicinity of Shih-Kang dam, the combined influence of the knickpoint and dam leads to aggradation upstream of the reservoir, accompanied by fining and narrowing of the channel (Fig. 6F and G). Within the incising zone downstream of the reservoir, the channel also widened; grain sizes at most downstream locations coarsened.

In the aggrading zone (upstream of 50 km), the areas both upstream and downstream of the Mar-An dam (built in 1997 at location E in Figs. 2B and 6D) exhibit substantial aggradation. In the most upstream area, high sediment supply from landslides after 2003 led to local profile aggradation > 20 m. Although, channel widths did not

Fig. 6. (A) Locations of 134 cross section locations (red lines with every 10th cross section number identified) surveyed by WRA from 1993 to 2008). Red channel boundary lines are WRA river basin management plan boundaries, and black lines represent locations of constructed levees. Yellow outline and slash areas are the locations of villages. (B) Longitudinal river profiles illustrated by different symbols from the year 1904 to 2008, showing locations of Shih-Kang reservoir (location F), Mar-An dam (location E), and Tien-Loon dam. (C) River channel slope, 1904 to 2008. Notice the knickpoint at Shih-Kang reservoir at the Chelungpu fault, located at about 23 km. (D) Normalized elevation variations for decadal-scale data normalized by the year 1993 data for region downstream of the dashed line (51 km) and normalized by the year 2003 data for upstream locations. Point E is Mar-An dam position. Segments A, B, and C are the range of aerial photos in Fig. 9A, B, and C, respectively. (E) Century-scale data normalized by the year 1904 data for elevations downstream of dashed line (53 km) and by the year 2003 data for upstream elevations. The red error bars show the variations; cross symbol means the average value and the upper and lower error bar limits in the maximum and minimum values. Point F is the position of the Shih-Kang reservoir. (F) River channel width differences in the year 2000, 2005, and 2008; all of these channel width values have been normalized by the year 1998 channel width data. (G) Mean grain size data from the year 1983 and 2008; the dashed line indicates the location of Shih-Kang reservoir (F).

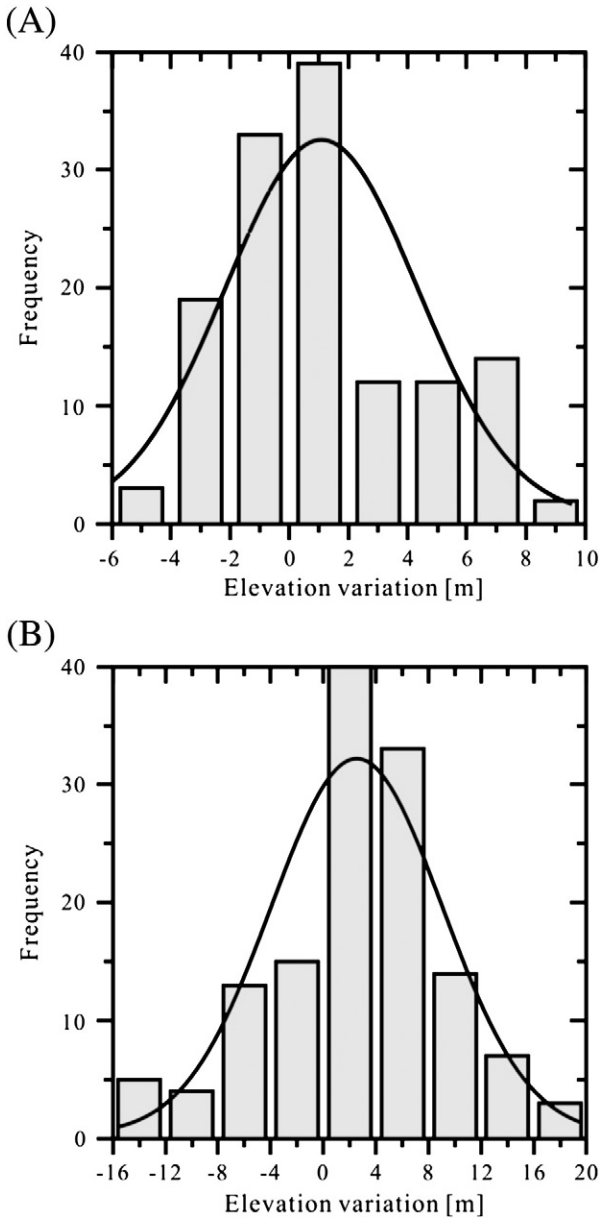

Fig. 8. Histograms of channel bed elevation variation and fitted normal distribution (black curve) in decadal-scale and century-scale comparisons. (A) Decadal-scale bed elevation data fit by a normal distribution with a mean value of 1.10 m and standard deviation of 3.28 m. (B) Century-scale bed elevation data fit by a normal distribution with a mean value of 2.60 m and standard deviation of 6.67 m.

change very much, a pronounced coarsening is apparent in data immediately downstream of Mar-An dam (Fig. 6F and G).

The century-scale profile analysis revealed basin-wide aggradation, with the exception of locations immediately upstream and downstream of Shih-Kang reservoir (Fig. 6B). As a result of the Chi-Chi earthquake the river profile was uplifted over a roughly 5 km reach upstream of Shih-Kang reservoir. Since 1904, incision occurred immediately downstream of Shih-Kang reservoir, and the channel bed has significantly aggraded upstream of Shih-Kang reservoir (30 km). Localized zones of substantial (>10 m) century-scale aggradation (4.5–10 km) and incision (11–15 km) are also apparent in the downstream reaches. This pattern may reflect extensive human modifications in these reaches where, according to WRAP (2010), railway bridges, levees, and farmland were built and developed in the early twentieth century.

Aerial photographs of reaches A, B, and C in 1975, 1988, and 2005 show channel response to sediment delivery and human impacts (see Fig. 6D). In reach C (Fig. 9C), the channel widened significantly after 1988 and upstream of the Shih-Kang reservoir the channel widened substantially from 2000 to 2008. Immediately downstream of Shih-Kang reservoir, in reach B (Fig. 9B), the channel narrowed significantly from 1975 to 1988 and then widened dramatically by 2005, presumably from breaching of the reservoir during the Chi-Chi earthquake. Reach A exhibited substantial channel widening from 1975 to 2005, despite overall bed incision after 2003.

While channel widening from 1975 to 2005 implies increased upstream sediment delivery to the river channel (Fig. 9), average channel width increased after 2000 (Table 4), implying a substantial increase in sediment supply. The average channel width increased by just 2 m from 1998 to 2000, after the Chi-Chi earthquake. However, channel width increased up to 68 m after the Haitang typhoon in 2005. The high intensity precipitation during typhoons provides the energy to deliver the sediment to the Tachia River channel. In addition, the average bed-surface grain size increased 12 mm from 1983 to 2008 (Fig. 6G). The increase in grain size from 1983 to 2008 downstream of Mar-An dam and Shih-Kang reservoir likely reflects the impact of dam construction.

4.3.4. Suspended sediment load variations

Evaluating the relative roles of typhoon precipitation and the impact of the Chi-Chi earthquake on sediment delivery and transport is difficult because suspended load data is available for a single hydrometric station along the Tachia River, Pai-Lu bridge station (1420H037). Since the suspended sediment data span the period from 1978 to 2003, we sorted these data into three periods: 1978 to 1989, 1990 to 1999, and 2000 to 2003 (post-Chi-Chi earthquake). Data from the period 2000–2003 exhibit a higher suspended sediment load than data from1990 to 1999, suggesting a post-earthquake effect, as argued by others for catchments in the epicentral region (Dadson et al., 2004, 2005; Chuang et al., 2009; Hovious et al., 2011). However, data from the period 1978–1989 likewise exhibit a systematically higher suspended sediment record than for the period from 1990 to 1999. Moreover, the highest sediment concentrations occurred during this period, not after the Chi-Chi earthquake. The higher post-earthquake suspended sediment loads at low discharges ($<20\ m^3\ s^{-1}$) suggest increased post-earthquake sediment availability in rivers in the Tachia catchment (e.g., Goldsmith et al., 2008). Given the overlap in the suspended sediment rating curves for the 1978 to 1989 and the post-earthquake periods for high flows ($>100\ m^3\ s^{-1}$), the hypothesized post-earthquake enhancement of sediment delivery is most conspicuous at low flows between typhoon events (Fig. 10).

4.3.5. Reservoir sedimentation records

Changes in reservoir sediment volumes over time can be used to track catchment sediment delivery (Rowan et al., 1995; White et al., 1997; Foster et al., 2007; Foster, 2010). Reservoir data are available at six widely distributed locations along the Tachia River. Reported sediment grain size for reservoir sediment deposits (Table 5) indicate coarse (bedload) deposition in downstream reservoirs (Mar-An) and fine (suspended load) sediment in the upstream most dam (Tehchi). The earliest dam was constructed in 1961, providing up to a half century of data (Fig. 11A). We divided the sediment volumes reported for each reservoir by the incremental drainage area between each reservoir and the next one upstream to evaluate the erosion rate in each reservoir over annual and decade timescales (Fig. 11A and B). We also analyzed the average erosion rate over the total upstream drainage area for each reservoir (Table 5). Incremental drainage areas were adjusted to account for different construction times of each reservoir.

The fastest rate of sediment accumulation in Ku-Kuan reservoir occurred in 1961–1963 and 1970–1973, before construction of the upstream Tehchi reservoir. After the Chi-Chi earthquake, high erosion rates according to reservoir sedimentation records (Fig. 11A) were reported for the Shih-Kang and Teschi reservoirs, the upstream most

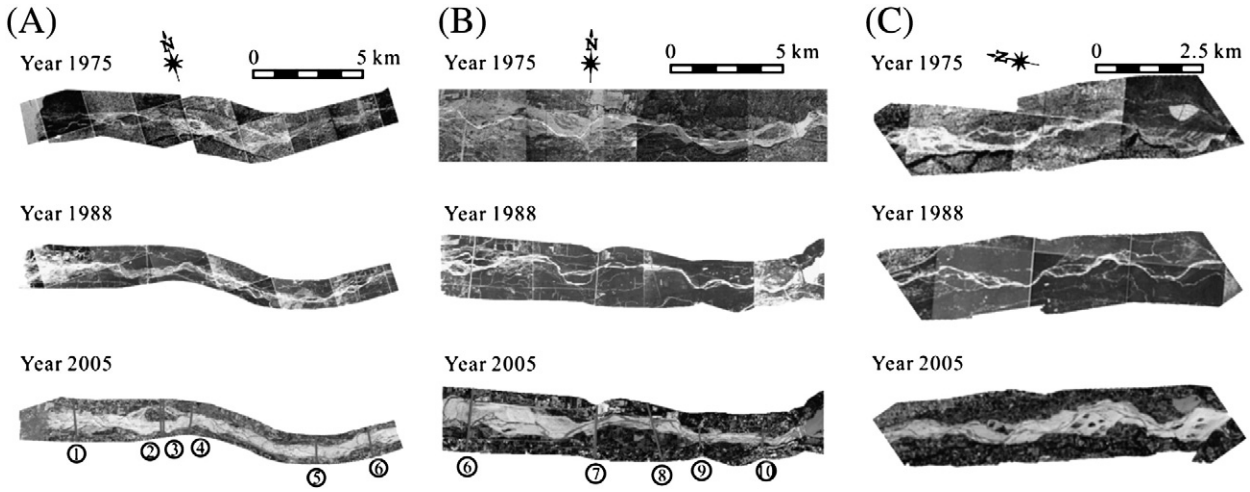

Fig. 9. Aerial photographs from 1975, 1988, and 2005 for three reaches of the Tachia River (locations shown in Fig. 6D). (A) Reach A extending from Chungshan highway bridge (bridge 6) to river mouth; six bridges are contained in this region. (B) Reach B, the region between Shih-Kang reservoir and Chungshan highway bridge (bridge 6); five bridges are contained in this area. (C) Reach C, the area from Tungshin bridge to Lungan bridge.

Table 4
The variation of average river channel width in Fig. 6F for the period from 1998 to 2008.

Year	1998	2000	2005	2008
Channel width [m]	443	441	511	508

and downstream most reaches, respectively. After Toraji typhoon (2001) the upstream Chinshan dam's erosion rate increased, and after typhoons Mindulle (2004) and Haitang (2005), sediment volume increased tremendously at the upstream most reservoir, Tehchi reservoir (to the right of dashed line in Fig. 11A). A significant increase in reservoir sedimentation rate after 2005 is apparent in the annual data from Tehchi, Mar-An, and Shin-Kang reservoirs.

The decade-averaged (decadal scale) erosion rates in each reservoir did not uniformly increase before and after the Chi-Chi earthquake (Fig. 11B). For example, the highest erosion rate at the Ku-Kuan reservoir occurred before 1980, but occurred in the 1980s and 1990s at the Tien-Loon dam.

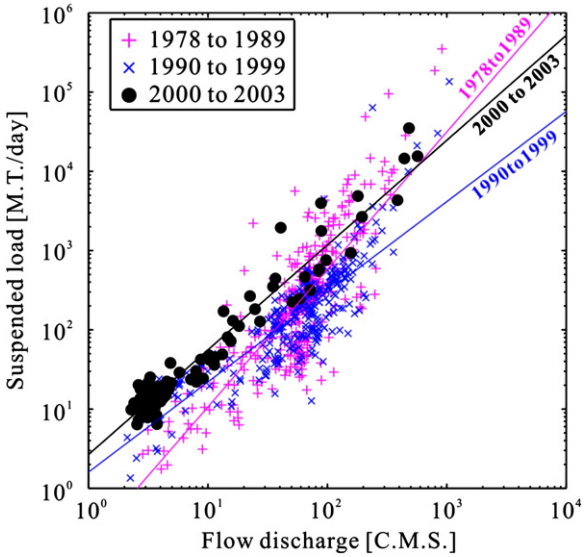

Fig. 10. Suspended sediment data from the hydrometric station, Pai-Lu bridge station (1420H037, location shown in Fig. 2D) showing data for the years 1978–1989, 1990–1999, and 2000–2003 (post-Chi-Chi earthquake).

We further examined the average decadal erosion rates by a weighted average of all six reservoir's drainage area based on both incremental and total drainage areas (Fig. 11C; Table 5). These two measures reflect differing constraints on sediment transport and reservoir trap efficiency; bedload sediment is unlikely to pass through a reservoir, whereas at least some suspended sediment is likely to do so. Before the Chi-Chi earthquake, reservoir sediment erosion rate was consistently under 1 mm y^{-1} when calculated using the total upstream drainage area, and under 2 mm y^{-1} when calculated using the incremental drainage area between one dam and the next (Fig. 11C). Reservoir sedimentation increased three-fold after the earthquake, from 0.4 mm y^{-1} for 1990–2000 to 1.4 mm y^{-1} after year 2000 for total drainage area, and from 1.8 mm y^{-1} to 6.2 mm y^{-1} for incremental drainage area. Most of the highest erosion rate records were contributed after Mindulle typhoon (2004) (Fig. 11A and C).

Long-term rainfall records from Taichung rainfall station (for the period 1897–2010), show that the decade-averaged maximum daily rainfall after 2000 was greater than in the period from 1960 to 2000. Decade-averaged erosion rates track decadal maximum daily rainfall (Fig. 12). The greater frequency of high intensity rainstorms in the post-earthquake period helps to explain the high erosion rates in the post-earthquake period.

5. Discussion and conclusions

Episodic processes triggered by earthquakes and typhoons deliver tremendous amounts of sediment from landslide-induced mass wasting in the drainage basin of the Tachia River. However, the different acquisition

Table 5
Drainage areas and deposited sediment particle sizes for the six reservoirs shown in Fig. 2B.

Reservoirs	Drainage area [km^2]		Date Built	D_{50} [mm]	D_{90} [mm]
	Total	Incremental			
A. Tehchi	592.0	592.0	1973	0.0083[a]	–
B. Chinshan	595.8	3.8	1970	–	–
C. Ku-Kuan	686.0	90.2	1961	–	–
D. Tien-Loon	827.0	141.0	1963	–	–
E. Mar-An	916.4	89.4	1997	12.5[a]	75[a]
F. Shih-Kang	1061.0	144.6	1977	0.2[a]	0.33[a]

'–' means no data.
[a] Particle size data from WRA (2010).

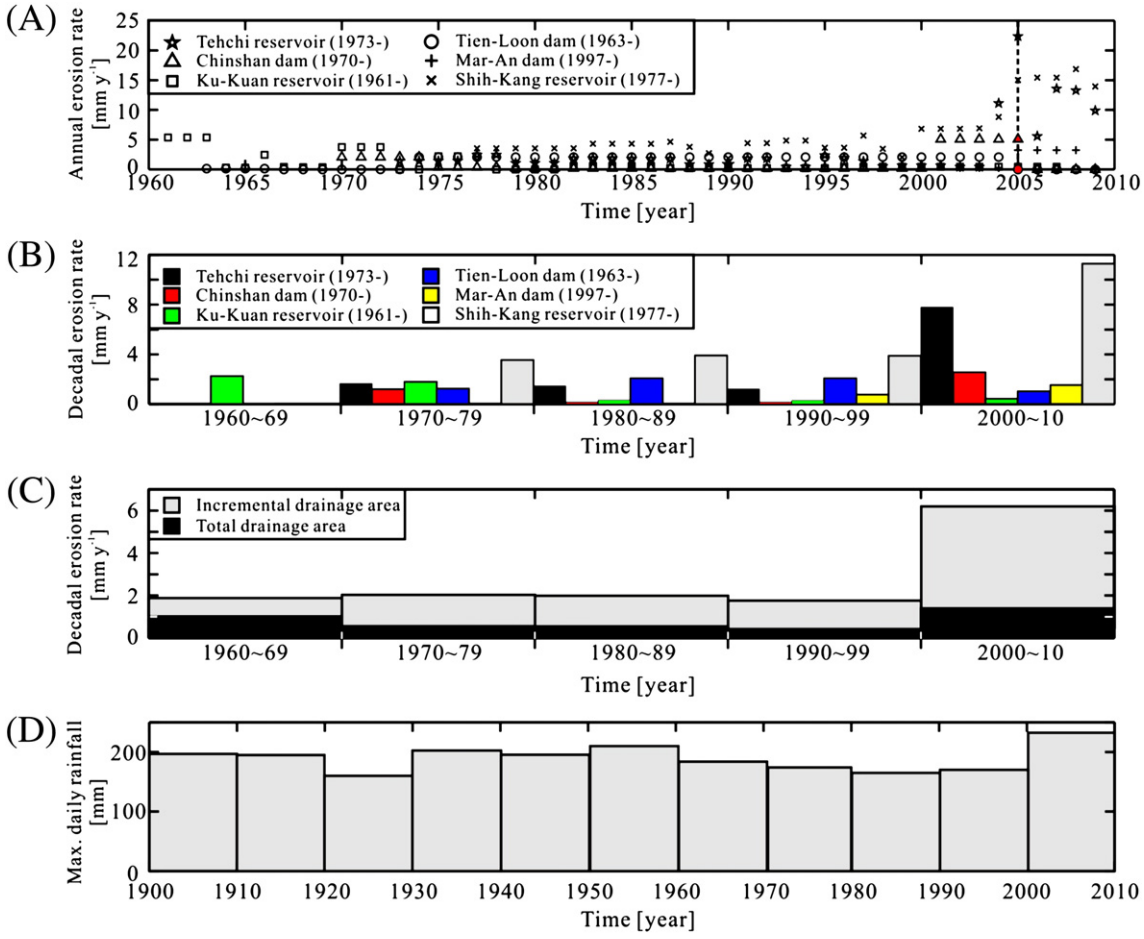

Fig. 11. Sediment data from six reservoirs along the Tachia River. (A) The annual erosion rates based on reservoir sediment for 1960 to 2010. The legend shows the symbols and the dam construction times. The red line shows the timing of the Haitang typhoon (2005). (B) A bar graph displays the average decadal erosion rate in each reservoir ordered from upstream (left) to downstream (right) for each decade. (C) Bar graph of the average erosion rate in the drainage basin of the Tachia River; dark black bar is calculated using accumulated drainage area, and gray bar data is calculated using the incremental drainage area. (D) Century-scale average maximum daily rainfall records from Taichung rainfall station (location shown in Fig. 1).

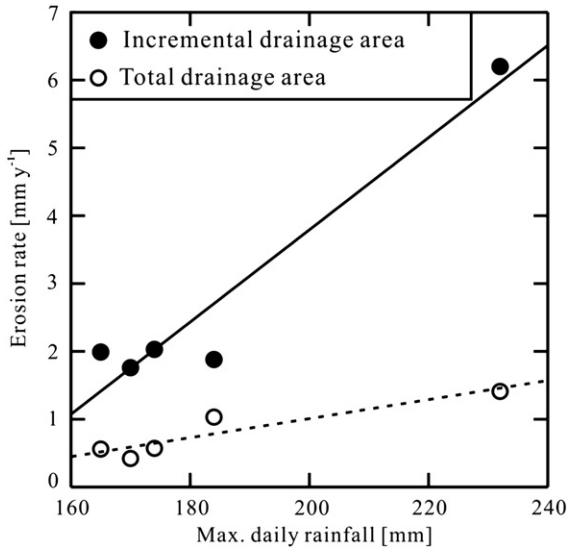

Fig. 12. The relationship between decadal-scale average maximum daily rainfall records (DR) and decadal-average erosion rata (ER) of all reservoirs from 1960 to 2010. Solid black circles are data evaluated by incremental drainage areas and the hollow circle data were based on the accumulated drainage areas. The solid black line is the linear fitting result of all incremental drainage areas data (regression equation: $ER = 0.068 \cdot DR - 9.81$, $R^2 = 0.93$). The accumulated drainage area data is also fit by linear regression as shown by the black dashed line (regression equation: $ER = 0.014 \cdot DR - 1.80$, $R^2 = 0.87$).

times of the satellite images and aerial photographs used to identify landslides triggered by the Chi-Chi earthquake in some previous studies make it difficult to unambiguously distinguish co-seismic and post-seismic failures because both the earthquake and significant storms happened during this time period, a problem highlighted by Wasowski et al. (2011) in a recent review of research on earthquake-induced landslides. For example, according to the SWCB Chi-Chi earthquake landslide database, most of the seismically induced landslides occurred along the Chelungpu fault and were not related to specific rock formations. While the studies of Khazai and Sitar (2003), Lin and Tung (2003), and Wang et al. (2003) supported this result, those of Chen (2009) and Chuang et al. (2009) came to a different conclusion based on their use of different landslide image time periods that overlapped significant storm events. However, based on our re-analysis we infer that the post-earthquake landslides (PEL) identified in the latter studies included a preponderance of storm-induced landslides between Tehchi reservoir and Mar-An dam.

Typhoon-induced landslide erosion rates exhibit a high degree of variability between catchments, but rock type appears to be a major control. Typhoon-induced landslides are strongly related to the spatial extent of Oligocene-age rock in the Tachia River basin. The observation of few earthquake-induced landslides in the Oligocene-age rock in the SWCB Chi-Chi earthquake landslide database likely reflects the influence of its greater rock strength than other geological units in the drainage basin. In addition, local weathering and development of near-surface fractures may promote failure of the Oligocene-age rock during pore-pressure elevating typhoon events.

Hillslope erosion rates by landsliding far exceed the downstream sediment delivery measured by reservoir sedimentation, indicating substantial storage of landslide-produced material on hillslopes (e.g., partial mobilization) and along headwater channels. The high fluvial sediment loading of the Tachia River is reflected in the nearly straight longitudinal profile and high-amplitude elevation fluctuations. Channel bed elevation and width have exhibited significant local changes to increased sediment delivery. The wider average river width and high reservoir sediment deposit volume after typhoon Mindulle in 2004 confirm that storm-triggered sediment delivery contributed most of the aggradation within the river channel. Over a decadal timescale, the river bed incised in the downstream reaches and aggregated in upstream reaches, a pattern consistent with the century-scale sediment transport and residence times predicted by Yanites et al. (2010) in rivers south of the Tachia basin. River engineering and flood control planning should expect substantial (>3 m) century-scale and (>1 m) decadal-scale variations in river bed elevations, a finding that has major implications for flood control strategies.

The relationship between channel morphology and sediment grain size proposed by Dade and Friend (1998), predicts that the downstream reaches of the Tachia River are bedload dominated. While high flows carry most of an increased suspended sediment load farther downstream, an increase in bedload would trigger aggradation in the river channel. The coarse grain sizes from 1983 to 2008 apparent in many reaches support the interpretation that bedload sediment accounted for the channel elevation fluctuations apparent in the century-scale and decadal-scale data. The grain-size coarsening immediately downstream of the Shih-Kang reservoir implies that the reservoir reduced downstream transmission of bedload. The high suspended sediment loads apparent in the early (i.e., 1978–1989) decadal scale suspended sediment records show that the high sediment yield potential of the Tachia catchment does not depend on earthquake-induced landsliding. Moreover, the reservoir sediment data show a greater increase in sediment delivery in the second half of the decade after the Chi-Chi earthquake, rather than a decay in sediment delivery during subsequent typhoons. Thus, it appears that in the Tachia River basin the proximal mechanism responsible for sediment delivery to the headwater channel system is high intensity precipitation.

According to century-long maximum daily rainfall records (Taichung rainfall station, Fig. 11D), the decade-averaged maximum daily rainfall after 2000 was the highest recorded since 1900, a factor consistent with secular climate change characteristics in Taiwan since 1900 (Hsu and Chen, 2002). That high intensity, short-duration rainstorms controlled sediment delivery is supported by the reservoir sediment deposition data.

Although researchers studying the epicentral region of the 1999 Chi-Chi earthquake report that earthquake effects influenced landsliding and sediment delivery during subsequent typhoons (Koi et al., 2008; Lin et al., 2008), triggering factors reported in previous studies (earthquake versus typhoon) are difficult to separate for the Tachia River basin. Nonetheless, the substantial quantities of river sediment produced by upstream landslides link river response to the sequence of earthquakes and typhoon events, producing significant bed profile fluctuations over decadal and century timescales. While different portions of the river are responding to fundamentally different forcing at present, the far greater hillslope erosion rates than the erosion rates inferred from observed reservoir sedimentation indicate that abundant sediment mobilized since the Chi-Chi earthquake remains in the catchment system, and documents the potential for sustained variability in fluvial response to the combination of strong tectonic activity and high intensity rainfall events that characterize western Taiwan.

Acknowledgments

We are grateful to the Taiwan Water Resources Planning Institute, TORI and TTFRI for sharing government reports and rainfall data of the Tachia River. Also, we would like to thank Prof. H.-H. Hsu, (Atmospheric Sciences, NTU) for sharing rainfall data and Prof. Marwan Hassan (UBC) for sharing suspended sediment data. Constructive comments by Richard Marston and the three anonymous reviewers significantly improved the manuscript.

References

Bureau of Energy (Ministry of Economic Affairs), 2009. General information of hydro power plant in Tachia river. Energy Monthly 1, 22–26 (in Chinese).
Chen, C.Y., 2009. Sedimentary impacts from landslides in the Tachia River basin, Taiwan. Geomorphology 105, 355–365.
Chen, C., Hawkins, A.B., 2009. Relationship between earthquake disturbance, tropical rainstorms and debris movement: an overview from Taiwan. Bulletin of Engineering Geology and the Environment 68, 161–186.
Chen, W.-S., Chen, Y.-G., Chang, H.-C., 2001. Paleoseismic study of the Chelungpu fault in the Mingjian area. Western Pacific Earth Sciences 1, 351–358.
Chen, W.-S., Chen, Y.-G., Shih, R.-C., Liu, T.-K., Huang, N.-W., Lin, C.-C., Sung, S.-H., Lee, K.-J., 2003. Thrust-related river terrace development in relation to the 1999 Chi-Chi earthquake rupture, western foothills, central Taiwan. Journal of Asian Earth Sciences 21, 473–480.
Chen, Y.C., Sung, Q., Chen, C.N., Jean, J.S., 2006. Variations in tectonic activities of the central and southwestern foothills, Taiwan, inferred from river hack profiles. Terrestrial Atmospheric and Oceanic Sciences 17, 563–578.
Cheng, C.T., Lin, Y.S., Ku, C.Y., Shu, S.M., Chang, Y.L., Yu, S.H., Yang, S.D., 2006. Application of remote sensing on hazardous landslides — a case study of Tachia river. Proceeding of the Conference of Chinese Geophysical Society. Chinese Geophysical Society, Jungli, Taiwan, pp. 1–13 (in Chinese).
Cheng, C.-T., Chiou, S.-J., Lee, C.-T., Tsai, Y.-B., 2007. Study on probabilistic seismic hazard maps of Taiwan after Chi-Chi earthquake. Journal of GeoEngineering 2, 19–28.
Chiou, S.-J., Cheng, C.-T., Hsu, S.-M., Lin, Y.-H., Chi, S.-Y., 2007. Evaluating landslides and sediment yields induced by the Chi-Chi earthquake and followed heavy rainfalls along the Ta-chia River. Journal of GeoEngineering 2, 73–82.
Chuang, S.C., Hongey, C., Lin, G.W., Lin, C.W., Chang, C.P., 2009. Increase in basin sediment yield from landslides in storms following major seismic disturbance. Engineering Geology 103, 59–65.
CWB (Central Weather Bureau), 2010. Historical typhoon data. http://photino.cwb.gov.tw/tyweb/mainpage.htm2010.
Dade, W.B., Friend, P.F., 1998. Grain-size, sediment-transport regime, and channel slope in alluvial rivers. Journal of Geology 106, 661–675.
Dadson, S.J., Hovious, N., Chen, H., Dade, W.B., Hsieh, M.L., Willett, S.D., Hu, J.C., Horng, M.J., Chen, M.C., Stark, C.P., Lague, D., Lin, J.C., 2003. Links between erosion, runoff variability and seismicity in the Taiwan orogeny. Nature 426, 648–651.
Dadson, S.J., Hovius, N., Chen, H., Dade, W.B., Lin, J.C., Hsu, M.L., Lin, C.W., Horng, M.J., Chen, T.C., Milliman, J., Stark, C.P., 2004. Earthquake-triggered increase in sediment delivery from an active mountain belt. Geology 32, 733–736.
Dadson, S., Hovius, N., Pegg, S., Dade, W.B., Horng, M.J., Chen, H., 2005. Hyperpycnal river flows from an active mountain belt. Journal of Geophysical Research 110, F04016, http://dx.doi.org/10.1029/2004JF000244.
Foster, I.D.L., 2010. Lakes and reservoirs in the sediment cascade. In: Burt, T., Allison, R. (Eds.), Sediment Cascades: An Integrated Approach. John Wiley and Sons, Chichester, UR, pp. 345–376.
Foster, I.D.L., Boardman, J., Keay-Bright, J., 2007. The contribution of sediment tracing to an investigation of the environmental history of two small catchments in the uplands of the Karoo, South Africa. Geomorphology 90, 126–143.
Goldsmith, S.T., Carey, A.E., Lyons, W.B., Kao, S.-J., Lee, T.-Y., Chen, J., 2008. Extreme storm events, landscape denudation, and carbon sequestration: typhoon Mindulle, Choshui River, Taiwan. Geology 36, 483–486.
Hack, J.T., 1973. Stream-profile analysis and stream-gradient index. Journal of Research of the U.S. Geological Survey 1, 421–429.
Hovious, N., Meunier, P., Lin, C.W., Chen, H., Chen, Y.G., Dadson, S., Horng, M.J., Lines, M., 2011. Prolonged seismically induced erosion and the mass balance of a large earthquake. Earth and Planetary Science Letters 304, 347–355.
Hsu, H.-H., Chen, C.-T., 2002. Observed and projected climate change in Taiwan. Meteorology and Atmospheric Physics 79, 87–104.
Keefer, D.K., 1984. Landslides caused by earthquakes. Bulletin of the Geological Society of America 95, 406–421.
Khazai, B., Sitar, N., 2003. Evaluation of factors controlling earthquake-induced landslides caused by Chi-Chi earthquake and comparison with the Northridge and Loma Prieta events. Engineering Geology 71, 79–95.
Koi, T., Hotta, N., Ishigaki, I., Matuzaki, N., Uchiyama, Y., Suzuki, M., 2008. Prolonged impact of earthquake-induced landslides on sediment yield in a mountain watershed: the Tanzawa region, Japan. Geomorphology 101, 692–702.
Korup, O., McSaveney, M.J., Davies, T.R.H., 2004. Sediment generation and delivery from large historic landslides in the Southern Alps, New Zealand. Geomorphology 61, 189–207.
Kuo, S.-J., Liu, K.-K., 2001. Estimating the suspended sediment load by using the historical hydrometric record from the Lanyang-Hsi watershed. Terrestrial Atmospheric and Oceanic Sciences 12, 401–414.
Larsen, I.J., Montgomery, D.R., Korup, O., 2010. Landslide erosion controlled by hillslope material. Nature Geoscience 3, 247–251.
Lee, J.-C., Chan, Y.-C., 2007. Structure of the 1999 Chi-Chi earthquake rupture and interaction of thrust faults in the active fold belt of western Taiwan. Journal of Asian Earth Sciences 31, 226–239.

Lee, C.-S., Tsai, L.L., 2010. A quantitative analysis for geomorphic indices of longitudinal river profile: a case study of the Choushui River, central Taiwan. Environmental Earth Sciences 59, 1549–1558.
Lee, Y.H., Lu, S.T., Shih, T.S., Hsieh, M.L., Wu, W.Y., 2005. Structures associated with the northern end of the 1999 Chi-Chi earthquake rupture, central Taiwan: implications for seismic-hazard assessment. Bulletin of the Seismological Society of America 95, 471–485.
Lin, M.L., Tung, C.C., 2003. A GIS-based potential analysis of the landslides induced by the Chi-Chi earthquake. Engineering Geology 71, 63–77.
Lin, M.L., Wang, K.L., Chen, T.C., 2000. Characteristics of the slope failure caused by the Chi-Chi earthquake. International Workshop on Annual Commemoration of Chi-Chi earthquake, September 18–20, vol. 3. National Centre for Earthquake Engineering, Taipei, Taiwan, pp. 199–209.
Lin, C.-W., Liu, S.-H., Lee, S.-Y., Liu, C.-C., 2006. Impacts of the Chi-Chi earthquake on subsequent rainfall-induced landslides in central Taiwan. Engineering Geology 86, 87–101.
Lin, G.W., Chen, H., Hovious, N., Horng, M.J., Dadson, S., Meunier, P., Lines, M., 2008. Effects of earthquake and cyclone sequencing on landsliding and fluvial sediment transfer in a mountain catchment. Earth Surface Processes and Landforms 33, 1354–1373.
Meunier, P., Hovius, N., Haines, A.J., 2007. Regional patterns of earthquake-triggered landslides and their relation to ground motion. Geophysical Research Letters 34, L20408, http://dx.doi.org/10.1029/2007GL031337.
Montgomery, D.R., Buffington, J.M., 1998. Channel processes, classification, and response. In: Naiman, R., Bilby, R. (Eds.), River Ecology and Management. Springer-Verlag, New York, NY, pp. 13–42.
NCREE (National Center for Research on Earthquake Engineering), 2000. Investigation Report of the Geotechnical Hazard Caused by Chi-Chi earthquake, Taiwan, Taipei, Taiwan. (in Chinese).
Rădoane, M., Rădoane, N., Dumitriu, D., 2003. Geomorphological evolution of longitudinal river profiles in the Carpathians. Geomorphology 50, 293–306.
Rowan, J.S., Goodwill, P., Greco, M., 1995. Temporal variability in catchment sediment yield determined from repeated bathymetric surveys: Abbeystead reservoir, UK. Physics and Chemistry of the Earth 20, 199–206.
Schuerch, P., Densmore, A.L., McArdell, B.W., Molnar, P., 2006. The influence of landsliding on sediment supply and channel change in a steep mountain catchment. Geomorphology 78, 222–235.
Shen, Z.-M., 1994. Flow profile's preparation, debug and examination. Taiwan Association of Hydraulic Engineer Sicence 10, 114–132 (in Chinese).
Shin, T.C., Teng, T.L., 2001. An overview of the 1999 Chi-Chi, Taiwan, earthquake. Bulletin of the Seismological Society of America 91, 895–913.
Snow, R.S., Slingerland, R.L., 1987. Mathematical modeling of graded river profile. Journal of Geology 95, 15–33.
Sung, Q., Chen, Y.-C., Tsai, H., Chen, Y.-G., Chen, W.-S., 2000. Comparison study on the coseismic deformation of the 1999 Chi-Chi earthquake and long-term stream gradient changes along the Chelungpu fault in central Taiwan. Terrestrial Atmospheric and Oceanic Sciences 11, 735–750.
SWCB (Soil, Water Conservation Bureau), 2000. Soil and Water Conservation Bureau. GIS landslide data of Chi-Chi earthquake. (http://www.swcb.gov.tw/index.asp) Council of Agriculture, Nantou, Taiwan.
SWCB (Soil, Water Conservation Bureau), 2002. GIS landslide data of Toraji typhoon. Taiwan: (http://www.swcb.gov.tw/index.asp) Council of Agriculture, Nantou, Taiwan.
Wang, W.N., Wu, H.L., Nakamura, H., Wu, S.C., Ouyang, S., Yu, M.F., 2003. Mass movements caused by recent tectonic activity: the 1999 Chi-Chi earthquake in central Taiwan. The Island Arc 12, 325–334.
Wasowski, J., Keefer, D.K., Lee, C.-T., 2011. Toward the next generation of research on earthquake-induced landslides: current issues and future challenges. Engineering Geology 122, 1–8.
White, P., Labadz, J.C., Butcher, D.P., 1997. Reservoir sedimentation and catchment erosion in the Strines catchment, UK. Physics and Chemistry of the Earth 22, 321–328.
WRA, 2010. Reservoir Sediment Releasing Countermeasures Cope with Climate Change (1/2). Water Resources Agency, Taipei, Taiwan. (in Chinese).
WRAH (Water Resources Agency History Map website), 2010. http://webgis.sinica.edu.tw/map_wra/2010.
WRAP, 2005~2010. Review report on Dajia River training plan (Tien-Lun dam to River Mouth). Water Resources Planning Institute (Water Resources Agency, MOEA), Taichung, Taiwan. (in Chinese).
Wu, F.T., Rau, R.-J., Salzberg, D., 1997. Taiwan orogeny: thin-skinned or lithospheric collision? Tectonophysics 274, 191–220.
Yanites, B., Tuckey, G.E., Mueller, K.J., Chen, Y.G., 2010. How rivers react to large earthquakes: evidence from central Taiwan. Geology 38, 639–642.
Yue, L.-F., Suppe, J., Hung, J.-H., 2005. Structural geology of a classic thrust belt earthquake: the 1999 Chi-Chi earthquake Taiwan (Mw = 7.6). Journal of Structural Geology 27, 2058–2083.